Dalton Transactions

PAPER

View Article Online
View Journal | View Issue

Cite this: *Dalton Trans.*, 2015, **44**, 14272

Wet-chemical synthesis of different bismuth telluride nanoparticles using metal organic precursors – *single source vs. dual source* approach†

Georg Bendt,[a] Anna Weber,[a] Stefan Heimann,[a] Wilfried Assenmacher,[b] Oleg Prymak[a] and Stephan Schulz*[a]

Received 1st June 2015,
Accepted 15th July 2015

DOI: 10.1039/c5dt02072g

www.rsc.org/dalton

Thermolysis of the *single source precursor* $(Et_2Bi)_2Te$ **1** in DIPB at 80 °C yielded phase-pure Bi_4Te_3 nanoparticles, while mixtures of Bi_4Te_3 and elemental Bi were formed at higher temperatures. In contrast, cubic Bi_2Te particles were obtained by thermal decomposition of $Et_2BiTeEt$ **2** in DIPB. Moreover, a *dual source approach* (hot injection method) using the reaction of $Te(SiEt_3)_2$ and $Bi(NMe_2)_3$ was applied for the synthesis of different pure Bi–Te phases including Bi_2Te, Bi_4Te_3 and Bi_2Te_3, which were characterized by PXRD, REM, TEM and EDX. The influence of reaction temperature, precursor molar ratio and thermolysis conditions on the resulting material phase was verified. Moreover, reactions of alternate bismuth precursors such as $Bi(NEt_2)_3$, $Bi(NMeEt)_3$ and $BiCl_3$ with $Te(SiEt_3)_2$ were investigated.

Introduction

In modern society, we are surrounded by waste heat emitters such as combustion engines, electronic components and even the human body. Since the amount of emitted heat is often only small, utilization of this energy is laborious but possible by thermoelectric generators, TEG, which allow the conversion of thermal energy into electric energy and therefore provide a wear- and noiseless power source.[1] The efficiency of a thermoelectric material is given by the dimensionless figure of merit ($ZT = (\alpha^2\sigma/\lambda)T$), where α is the Seebeck coefficient, σ is the specific electrical conductivity, λ is the thermal conductivity as sum of the electronic λ_{el} and the lattice λ_{la} contribution and T the absolute temperature in Kelvin. Unfortunately, the transport coefficients are linked together and typically can't be optimized independently from each other. For instance, metals show high electrical and thermal conductivities, whereas both values are small for insulators such as ceramics. The best choices for technical applications are semiconducting materials with heavy elements due to their high effective masses. For technical applications near room temperature, Sb_2Te_3 and Bi_2Te_3 as well as the solid ternary solutions $(Sb_xBi_{1-x})_2Te_3$ are the most effective materials due to their high electrical conductivities and high Seebeck coefficients combined with glass-like low thermal conductivities.[2] The thermal conductivity of a given material can be further lowered by nanostructuring approaches, which result in an increased phonon scattering at grain boundaries smaller than the phonons mean free path.[3] As a consequence, intense research has been done on this field, leading to several preparation and optimization strategies.

Scheele *et al.* showed that nanosized Bi_2Te_3 particles can be synthesized in a two-step process by reducing bismuth acetate with oleylamine to elemental bismuth particles in dodecanthiole and further treatment with trioctyltellurophosphorane TOPTe, which is a widely used soluble Te-source, at 110 °C. The resulting rhombohedral bismuth-rich Bi_2Te_3-particles showed reduced thermal conductivity after SPS-treatment and a high power factor (5 μW K^{-2} cm^{-1}).[4] Modifying this general synthetic protocol also allowed the synthesis of $(Sb_xBi_{1-x})_2Te_3$ nanoparticles. Stavila *et al.* investigated the thermolysis of TOPTe and bismuth oleate and investigated the role of the reaction temperature on the resulting particle shape. As-obtained particles reached ZT values of 0.38 at room temperature.[5] Moreover, bismuth nitrate and TOPTe were thermolyzed in octadecene and oleic acid by Ruan *et al.*, resulting in the formation of hexagonal und rod-shaped particles,[6] while Borca-Tasciuc *et al.* obtained hexagonal Bi_2Te_3 plates from the reaction of $BiCl_3$ and TOPTe in thioglycolic acid in a microwave

[a]*Institute of Inorganic Chemistry and Center for Nanointegration Duisburg-Essen (CeNIDE), University of Duisburg-Essen, Universitätsstr. 5-7, D-45117 Essen, Germany. E-mail: stephan.schulz@uni-due.de; Fax: +44 0201 1833830; Tel: +44 0201 1834635*

[b]*Institute of Inorganic Chemistry, University of Bonn, Römerstr. 164, D-53117 Bonn, Germany*

†Electronic supplementary information (ESI) available: DSC studies, ^{1}H-NMR spectroscopy studies, Rietveld refinements, SAED pattern, SEM pictures. See DOI: 10.1039/c5dt02072g

assisted synthesis.[7] The resulting material, which was subatomically doped with sulphur, showed a remarkably high *ZT* value (1.1).

Even though TOPTe is a suitable Te-precursor for the solution-based synthesis of bismuth tellurides, alternative Te-precursors have been investigated. A promising candidate is bis(triethylsilyl)tellurane $(Et_3Si)_2Te$, whose general capability to serve as rather low-temperature Te-precursor for the deposition of Sb_2Te_3 and Bi_2Te_3 thin films by atomic layer deposition (ALD)[8] as well as for the wet-chemical synthesis of GeTe-nanoparticles[9] was recently demonstrated. In addition, bis(trimethylsilyl)tellurane $(Me_3Si)_2Te$ in combination with bismuth trisamides $Bi(NR_2)_3$ was also successfully applied as low-temperature MOCVD precursor for the deposition of Bi_2Te_3 thin films.[10] Surprisingly, to the best of our knowledge, an analogous solution-based synthesis of Bi_2Te_3 nanoparticles using these specific precursors has not yet been reported.

Bi_2Te_3 crystallizes in the tetradymite-type structure with five membered stacks of alternating tellurium and bismuth layers along the *c*-axis with the sequence Te^1–Bi–Te^2–Bi–Te^1, in which the indices correspond to tellurium atoms in different environments. Each stack has the composition Bi_2Te_3 and the hexagonal unit cell ($R\bar{3}m$: H) contains 3 formula units.[2] A general problem in the wet-chemical synthesis of Bi_2Te_3 nanoparticles is their strong tendency to form so-called antisite defects, the occupation of either Te sites by Bi atoms or Bi sites by Te atoms in the tetradymite lattice, resulting in the formation of either p- or n-doped materials. This well-known process strongly influences the carrier concentration and therefore the thermoelectric properties of the resulting material.[11] Moreover, the facile incorporation of excess bismuth into the tetradymite lattice leads to a series of sandwich-like structures of the general form $(Bi_2)_n(Bi_2Te_3)_m$, in which the quintuple layers are separated by Bi-bilayers[12] as can be observed in tsumoite BiTe, pilsenite Bi_4Te_3 and hedleyite Bi_7Te_3, respectively.

Single source precursors (SSPs), which contain the elements of the desired material already pre-formed in a single molecule, are promising alternative precursors for the synthesis of nanoparticles and thin films.[13] They are typically easier to handle, their thermal properties can be modified by the precursor design and they typically exhibit lower decomposition temperatures, which render them very attractive as low-temperature precursors. While the use of SSPs for the synthesis of several main group and transition metal chalcogenides[14] including M_2E_3 nanoparticles (M = Sb, Bi; E = S, Se) is well established,[15] suitable SSPs for Sb_2Te_3 have only been recently developed. Sb_2Te_3 nanoplates were obtained from aerosol assisted chemical vapor deposition (AACVD) using $[Sb\{(TeP^iPr_2)_2N\}_3]$.[16] In addition, $Ph_2SbTeEt$[17] and $MeSb(TeBu)_2$ [18] were recently shown to be promising SSPs for the wet-chemical synthesis of Sb_2Te_3 nanoparticles and the CVD deposition of Sb_2Te_3 thin films. While early AACVD studies with $Et_2SbTeEt$ and $Te(SbEt_2)_2$ failed to give Sb_2Te_3 films,[19] we successfully demonstrated the promising potential of $Te(SbEt_2)_2$ to serve as SSP for the solution based[20] and gas phase based[21] synthesis of highly stoichiometric Sb_2Te_3 nanoparticles and thin films with high Seebeck coefficients. These studies clearly demonstrated that the formation of antisite defects in Sb_2Te_3 nanoplates can be significantly reduced by use of this specific SSP. Moreover, the studies showed that the ligand design of the precursors is of high interest in order to control the specific decomposition mechanism and therefore the level of impurities incorporated into the resulting material. In remarkable contrast, *single source precursors* for the solution-based synthesis of high-quality Bi_2Te_3 nanoparticles have not been reported to the best of our knowledge, while Reid *et al.* recently demonstrated that the bismuth chloride telluroether complex $[BiCl_3(TeBu_2)_3]$ is a suitable *single source precursor* for the MOCVD deposition of high-quality Bi_2Te_3 thin films.[22]

Herein we report on our attempts to prepare suitable *single source* and *dual source precursors* for the wet-chemical synthesis of crystalline Bi_2Te_3 nanoparticles at rather mild reaction condition below 100 °C.

Results and discussion

Thermolysis of $(Et_2Bi)_2Te$ 1

Since $(Et_2Sb)_2Te$ was previously shown to exhibit superior properties as SSP for the solution-based synthesis of high-quality hexagonal Sb_2Te_3 nanoplates,[20] the heavier homologue $(Et_2Bi)_2Te$ **1**, which is readily accessible by insertion reaction of elemental Te into the weak Bi–Bi bond of tetraethyldibismuthine Et_4Bi_2 in *n*-pentane at low temperature,[23] was investigated.

1 is a red solid, whose thermal properties were studied by differential scanning calorimetry (DSC). The endothermic peak at 51.3 °C indicates the melting point of **1**, followed by a broad exothermic peak between 60 and 100 °C, corresponding to its thermal decomposition (ESI, Fig. S3†). From the resulting product mixture, Et_3Bi and Et_2Te were clearly identified. Et_3Bi (170 °C) and Et_2Te (225 °C) decompose at higher temperatures, which was confirmed by comparison with the DSC curves of the pure compounds (ESI Fig. S1 and S2†). These findings were confirmed by thermolysis studies of **1** in a sealed melting point capillary, showing melting of **1** at 53 °C followed by a colour change from red to black upon further temperature increase. In addition, Et_3Bi and Et_2Te were clearly identified as decomposition products of **1** in a thermolysis experiment in a sealed NMR-tube. According to these studies, the decomposition of **1** occurs by a different and more complex reaction mechanism, which most likely includes the formation of radicals, compared to that of $(Et_2Sb)_2Te$, which proceeded in a stoichiometric reaction with subsequent formation of Sb_2Te_3 and four equivalents of $SbEt_3$.[20]

The thermolysis reaction of **1** was performed with 200 mg $(Et_2Bi)_2Te$ **1**, which was dissolved in 10 mL DIPB, slowly heated to 170 °C and stirred for 1 h. The red solution turned into a black suspension around 80 °C. After cooling to ambient temperature, macroscopic, shiny metallic-like particles were isolated from the colourless liquid by centrifugation and were shown by EDX studies to consist of pure bismuth metal. The thermo-

lysis temperature was therefore lowered to 80 °C, yielding a black powder after work up. The chemical composition of the material as-determined by EDX analysis revealed a bismuth to tellurium ratio of 56 : 44 at%, which is close to the theoretical value for Bi_4Te_3 (57 : 43). All observed peaks in the PXRD pattern (Fig. 1) can be indexed on the basis of rhombohedral Bi_4Te_3 (JCPDS 33-216). The lattice parameters were refined to (a = 4.43(1) Å, c = 41.84(1) Å and V = 415.5(4) Å^3) (ESI Fig. S10.† The broad full width half maximum (FWHM) of the peaks indicate a small particle size of roughly 20 nm.

TEM studies of the nanoparticles (Fig. 2) show the formation of agglomerated particles of roughly 200 nm in size, consisting of smaller particles with diameter ranging from 10 to 40 nm. The particles are crystalline and lattice fringes of the randomly orientated crystals are easily resolved in HRTEM. A d-spacing of roughly 310 pm is often observed, which refers to the 100% peak (107) in the PXRD. The corresponding ring diffraction pattern (ESI Fig. 14†) from an area with several crystals is in good agreement with the PXRD result and proves the formation of crystalline Bi_4Te_3 nanoparticles by simulation[24] using 30526-ICSD.[25]

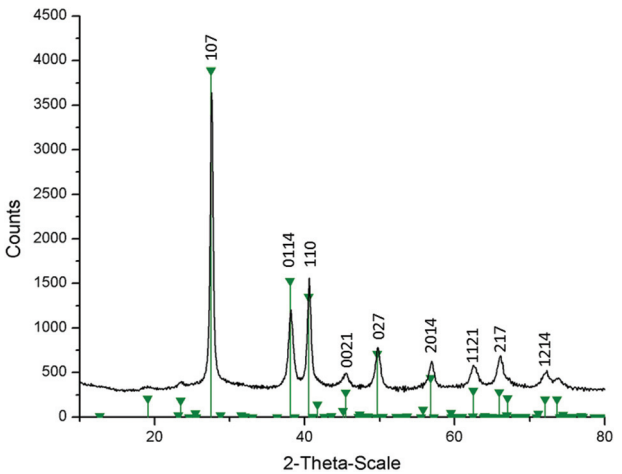

Fig. 1 X-ray diffractogram of Bi_4Te_3 nanoparticles as obtained by thermal decomposition of **1** at 80 °C in DIPB and reference (green: Bi_4Te_3, JCPDS 33-216).

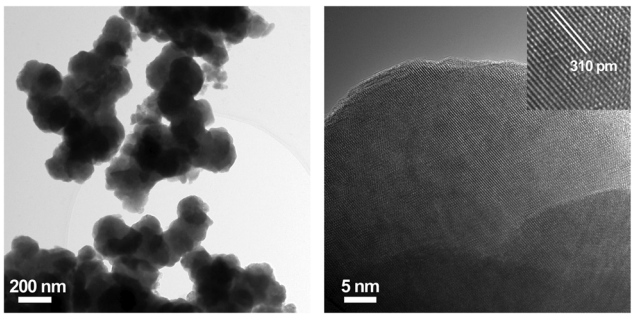

Fig. 2 TEM images of Bi_4Te_3 nanoparticles as obtained by thermal decomposition of **1** at 80 °C in DIPB.

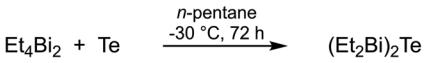

Scheme 1 Synthesis of **1**.

In an attempt to suppress the agglomeration of the particles, the thermolysis reaction of **1** according to Scheme 1 was performed at 80 °C in DIPB in the presence of 3 wt% of poly-(1-vinylpyrolidone)-*graft*-(1-triacontene) PVP* as capping agent. After workup, a black powder was obtained. TEM analysis of the powder showed less agglomeration and the size of the crystalline particles (Fig. 3) increased as can be seen by the diffraction contrast of the grains, which however showed no distinct morphology. The SAED (ESI Fig. S15†) pattern again corresponds well to the calculated pattern of Bi_4Te_3.

Thermolysis reactions at higher temperatures between 100 and 130 °C yielded mixtures of Bi_4Te_3 and elemental Bi as a second crystalline phase as was proven by PXRD (ESI, Fig. S18†). Analogous findings were observed for thermolysis reactions in this temperature range in DIPB in the absence of any capping agent. These findings show, that the decomposition mechanism of **1** and its lighter homologue $(Et_2Sb)_2Te$ strongly differ at enhanced temperatures, which most likely has its origin in the low Bi–Te bond energy, rendering homolytic bond cleavage with subsequent formation of radical species more likely.

Thermolysis of $Et_2BiTeEt$ 2

Since the decomposition of **1**, in which the Bi : Te ratio is 2 : 1, only yielded the Bi-rich binary bismuth–tellurium phase Bi_4Te_3 (pilsenite), we became interested in the thermal decomposition of a precursor with lesser amount of Bi. Et_2Bi-TeEt **2**, which was prepared by reaction of Et_4Bi_2 and Et_2Te_2,[26] was therefore chosen as promising *single source precursor* (Scheme 2).

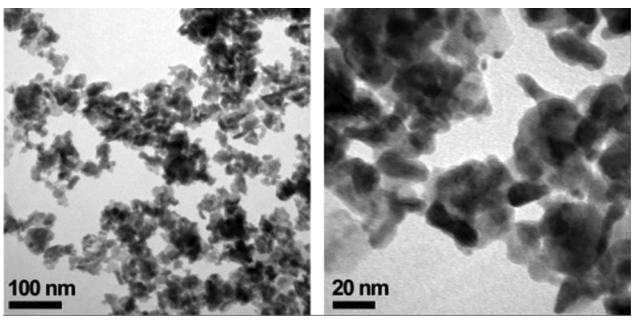

Fig. 3 TEM images of Bi_4Te_3 nanoparticles as obtained by thermal decomposition of **1** at 80 °C in DIPB in the presence of 3 wt% of PVP*.

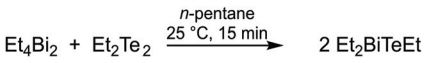

Scheme 2 Synthesis of **2**.

The reaction of Et_4Bi_2 and Et_2Te_2 in toluene-d_8 was monitored by temperature dependent ^{1}H-NMR spectroscopy (ESI, Fig. S5†). Below 75 °C, no reaction was observed, while new signals with growing intensity appeared at temperatures above 75 °C, proving the formation of $Et_2BiTeEt$ **2**, which decomposes at 85 °C with formation of Et_3Bi and Et_2Te as well as insoluble solid material (ESI; Fig. S6†). According to our DSC study (ESI, Fig. S4†), decomposition of **2** yields Et_3Bi and Et_2Te, which decompose at 270 °C and 225 °C, respectively.

Thermolysis reactions of **2** were performed in DIPB and in oleylamine (OA) for 3 and 14 h, respectively, in order to investigate the role of solvent and reaction time on the composition and morphology of the resulting material. For these studies, **2** was freshly prepared *in situ* by stirring a solution of Et_4Bi_2 and Et_2Te in the respective solvent at ambient temperature for 30 minutes, followed by heating to 100 °C for 14 h. The resulting black suspension was centrifuged and the black solid repeatedly washed (3×) with chloroform.

The chemical composition of resulting materials was analysed by EDX (Bi : Te ratio 65 : 35 at% (DIPB) and 62 : 38 at% (OA)). These results again show the formation of Bi-rich materials. X-ray diffraction studies confirmed the EDX results, proving the formation of phase-pure Bi_2Te in DIPB (Fig. 4), while the material formed in OA contained elemental Bi as second phase (ESI, Fig. S19†). Any attempts to increases the Te-content in the material by adding TOPTe as soluble Te-source failed. In all cases, Bi_2Te was formed as was proven by EDX and XRD, respectively.

SEM pictures of the resultant black particles proved the formation of pseudo-cubic particles with edge lengths of several 100 nm (Fig. 5). With increasing reaction time, the particle size increases to 500 nm, proving an Ostwald ripening of the initially formed nanoparticles.

In summary, all thermolysis reactions using **1** and **2** resulted in the formation of tellurium-poor phases, while Bi_2Te_3 was not formed. These findings point to different

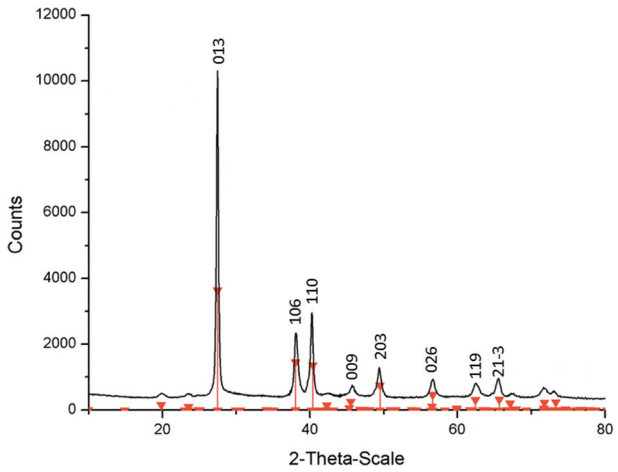

Fig. 4 X-ray diffractogram of black powders as obtained by thermal decomposition of **2** at 100 °C in DIPB and reference (red: Bi_2Te, JCPDS 42-540).

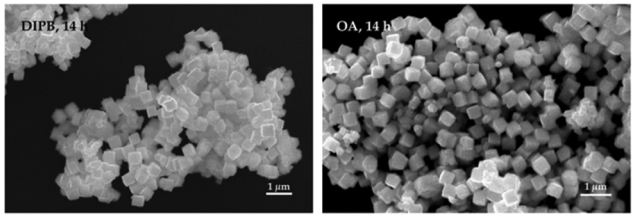

Fig. 5 SEM images of Bi_2Te nanoparticles as obtained by thermal decomposition of **2** at 100 °C in DIPB (a) and OA (b).

decomposition mechanisms of **1** and **2** compared to analogous antimony compounds as well as bismuth selenolates $(R_2Bi)_2Se$ and R_2BiSeR', which have been reported to decompose with formation of trialkylbismuthanes R_3Bi and Bi_2Se_3 or $RBi(SeR')_2$, respectively,[27] and may be attributed to the decreasing Bi–E bond energy with increasing atomic number of the chalcogen atom. Breunig *et al.* investigated the decomposition mechanism of **1** and **2** by mass spectroscopy and detected multiple species in the gas phase, indicating a complex decomposition mechanism.[28] According to Pauling's postulate, that heteronuclear bonding is always stronger than homonuclear bonding,[29] it seems reasonable to assume that the Bi–Te bond is the weakest bond within **1** and **2**, since the electronegativity difference between Bi and Te is less compared to that between Bi and C as well as Te and C. **1** and **2** are therefore expected to undergo homolytic Bi–Te bond breakage reactions, even though the corresponding metal-centered radicals have not been identified directly by ESR experiments to the best of our knowledge, to date. However, the same is true for tetraalkyldistibines and -dibismuthines, for which homolytic Sb–Sb and Bi–Bi bond cleavage reactions with subsequent formation of metal centered radicals are widely accepted, despite the lack of broad experimental proof. To the best of our knowledge, only one persistend Bi-centered radical, which was formed by a homolytic bond cleavage reaction of a dibismuthine containing sterically demanding organic substituents, was clearly identified.[30] In contrast, ESR experiments with Me_4Bi_2 as well as Ph_4Bi_2 failed to give signals due to the formation of Ph_2Bi radicals, even though reactivity studies agreed with their formation.[31]

Compounds of the type R_2BiTeR' have been previously described to decompose in solution at elevated temperature with formation of BiR_3 and $RBi(TeR')_2$, but mechanistic studies were not presented.[27,32] In contrast, our DSC and NMR studies using **1** and **2** only proved the formation of Et_3Bi and Et_2Te, while no indication for the formation of $EtBi(TeEt)_2$ was found. Any attempts to detect radical intermediates by addition of TEMPO to the reaction solution remained without success. We assume, that the formation of temperature stable Et_2Te, which was experimentally proven by DSC and NMR studies, is an efficient process for the transport of Te out of the reaction mixture, always resulting in the formation of Te-poor (Bi-rich) materials. However, the exact decomposition mechanism for the formation of Bi_4Te_3 or Bi_2Te using either **1**

or **2** as SSPs remain still unclear and are expected to depend on the specific organic substituents as was previously reported by Bochmann *et al.* for several tris-selenolato-bismuthines $Bi(SeR)_3$.[33] Thermal decomposition reactions of $Bi(SeR)_3$ in solution preferentially proceeded with formation of elemental Bi due to the favorable breakage of the Bi–Se bond compared to the Se–C bond. However, the decomposition mechanism was found to strongly depend on the organic substituents. $(2,4,6\text{-}t\text{-}Bu_3C_6H_2Se)_3Bi$ was found to decompose with elimination of the selenane R_2Se and formation of a mixture of elemental bismuth and Bi_2Se_3, while $(2,4,6\text{-}Me_3C_6H_2Se)_3Bi$ yielded elemental Bi and the diselenane R_2Se_2.

Reaction of $Bi(NMe_2)_3$ with $Te(SiEt_3)_2$

Since the thermal decomposition reactions of both *single source precursors* **1** and **2** failed to give the desired Bi_2Te_3 phase, we became interested in the development of a suitable *dual source approach*. ALD studies have revealed that $Bi(NMe_2)_3$ and $Te(SiEt_3)_2$ are suitable precursors for the formation of Bi_2Te_3 thin films,[10] so we expanded our studies on the reactions of $Bi(NR_2)_3$ and $Te(SiEt_3)_2$. Addition of $Bi(NMe_2)_3$ to a solution of $Te(SiEt_3)_2$ in DIPB at ambient temperature resulted in an immediate darkening, indicating a fast reaction. Monitoring the reaction in THF-d_8 by ^{1}H-NMR spectroscopy proved that the reaction proceeded with elimination of *N*,*N*-dimethylaminotriethylsilane Me_2NSiEt_3, which is the only detectable product after 15 minutes (ESI, Fig. S7†). According to these studies, the reaction occurs by the following mechanism (Scheme 3):

Influence of reaction temperature. Since the reaction temperature is known to play an important role for the formation of nanoparticles and has major impacts on size, shape and crystallinity of the resulting nanoparticles, we systematically varied the reaction temperature from 30 °C to 120 °C. PXRD studies of the resulting materials obtained at low temperatures showed broad peaks, which did not allow the detailed assignment of any specific phases, and SEM studies showed the formation of small particles with undefined morphology (Fig. 6).

With increasing reaction temperature, the peaks in the PXRDs became sharper, pointing to the formation of larger crystallites, and revealed Bi_2Te_3 to be present as dominate phase as well as small contributions of Bi_4Te_3 (Fig. 7). The SEM studies showed increasing particle size and a star-like morphology of the nanoparticles. EDX analysis revealed the formation of Bi-rich material (Bi : Te ratio 44 : 56 at%), which clearly deviates from the expected 40 : 60 ratio for phase-pure Bi_2Te_3.

Influence of thermolysis procedure and precursor ratio. Since only biphasic bismuth tellurides were formed as described before, the thermolysis conditions were slightly

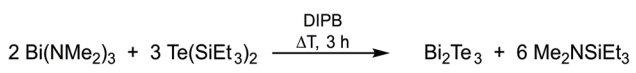

Scheme 3 Reaction of $Bi(NMe_2)_3$ and $Te(SiEt_3)_2$.

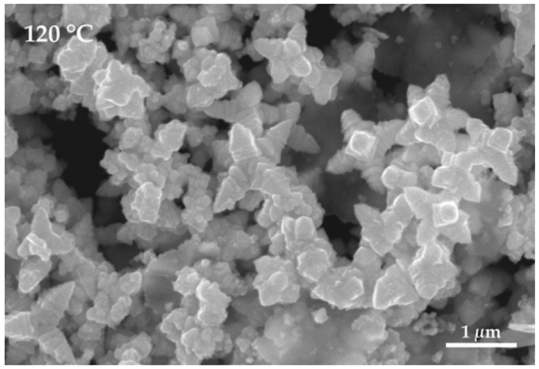

Fig. 6 SEM images of Bi_2Te_3 nanoparticles as obtained by reaction of $Bi(NMe_2)_3$ and $Te(SiEt_3)_2$ at 120 °C in DIPB.

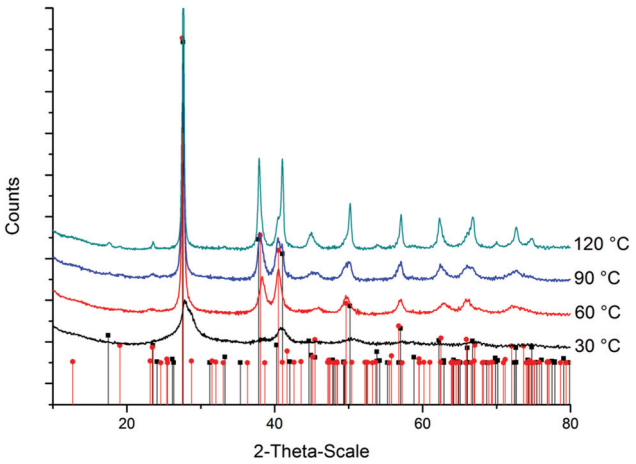

Fig. 7 X-ray diffractogram of black powders as obtained by reaction of $Bi(NMe_2)_3$ and $Te(SiEt_3)_2$ at different temperatures. Bi_2Te_3 (black: JCPDS 015-0863) and Bi_4Te_3 (red, JCPDS 33-216).

modified. The Te precursor was dissolved in DIPB and heated to 100 °C. $Bi(NMe_2)_3$ was then rapidly injected (hot injection) to this solution, immediately resulting in the formation of a black powder, which was isolated by centrifugation after 3 h. PXRD studies proved the formation of phase-pure Bi_2Te_3 (Fig. 8a) The refined lattice parameters for the nanosized Bi_2Te_3 particles as determined by Rietveld analysis (Fig. S11†) for Bi_2Te_3 (a = 4.399(1) Å, c = 20.297(3) Å and V = 507.7(1) Å^3) are in good agreement with values reported for Bi_2Te_3 (JCPDS 015-0863). Since a multiplicity of bismuth telluride phases with different bismuth concentration exists, we carefully investigated thermolysis reaction of $Bi(NMe_2)_3$ and $Te(SiEt_3)_2$ also with two different precursor molar ratios (1 : 1; 4 : 3). The solution of $Te(SiEt_3)_2$ in DIPB was heated to 100 °C, followed by addition of different amounts of a solution of $Bi(NMe_2)_3$ in DIPB, also yielding black suspensions, from which black powders were isolated by centrifugation after 3 h. Depending on the precursor ratio, two different phases with Bi : Te molar ratios of 1 : 1 (BiTe) and 4 : 3 (Bi_4Te_3) were obtained (Fig. 8b

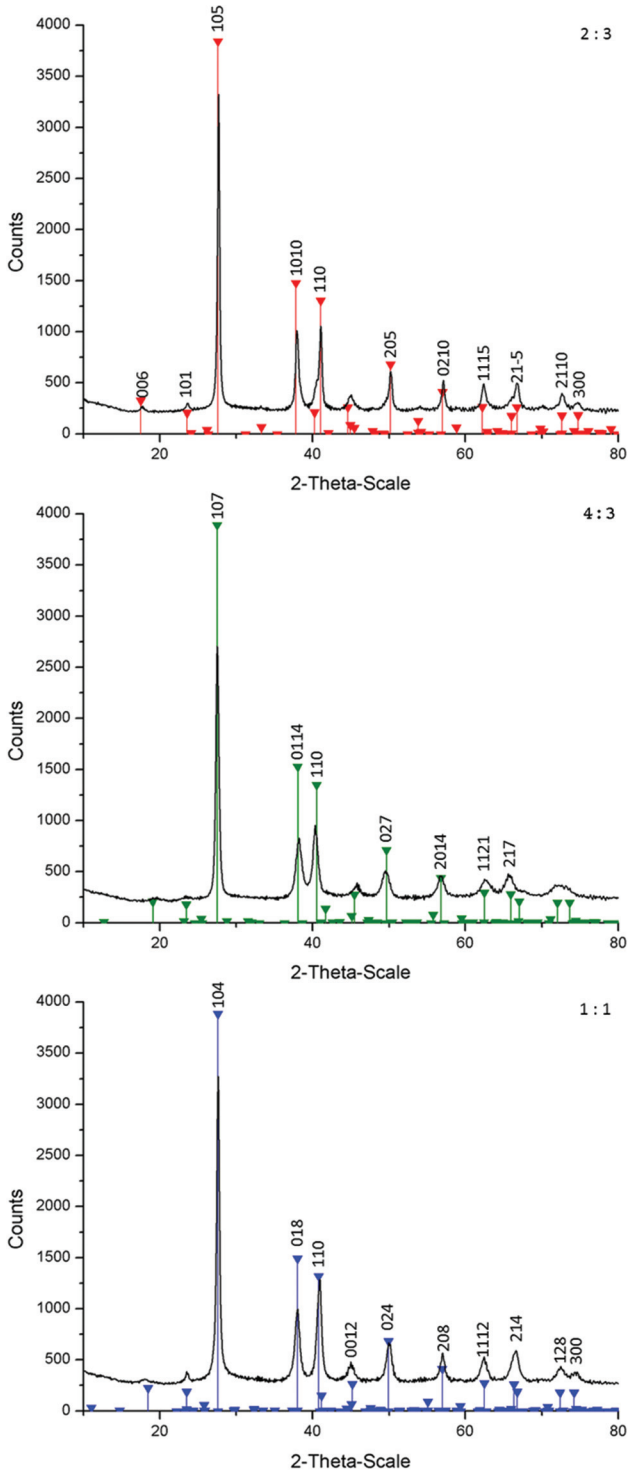

Fig. 8 X-ray diffractograms of black powders as obtained by reaction of $Bi(NMe_2)_3$ and $Te(SiEt_3)_2$ in DIPB in 2 : 3 (a), 4 : 3 (b) and 1 : 1 (c) molar ratios at 100 °C and references (red: Bi_2Te_3, JCPDS 015-0863; green: Bi_4Te_3, JCPDS 33-216; blue: BiTe, JCPDS 44-0667).

and c). In each case, the chemical composition is close to the theoretical value with respect to the experimental error. The refined lattice parameters for the nanosized particles as determined by Rietveld analysis for BiTe (a = 4.420(5) Å, c = 24.09(2) Å and V = 407.5(9) Å^3; Fig. S12†) and Bi_4Te_3 (a = 4.462(1) Å, c = 41.84(1) Å and V = 721.1(4) Å^3, Fig. S13†) are in good agreement with values reported in the literature for these binary bismuth–tellurium phases (JCPDS No. 015-0863 (Bi_2Te_3), No. 015-0863 (Bi_4Te_3) and No. 44-0667 (BiTe).

Since the formation of the desired Bi_2Te_3 phase was of particular interest, the particles were further analysed by TEM, showing small pseudo-cubic particles with edge lengths of roughly 40 nm (Fig. 9). The SAED pattern (Fig. S16†) of these particles is in good agreement with the literature data and clearly shows the formation of phase pure Bi_2Te_3 as proven by comparison with calculated ED-pattern using data from ICSD-42546.[34]

Fig. 10 displays a HRTEM image of a Bi_2Te_3 nanoparticle from $Bi(NMe_2)_3$ and $Te(SiEt_3)_2$ (2 : 3 molar ratio) in DIBP at 100 °C in [110] zone axis orientation, thus perpendicular to

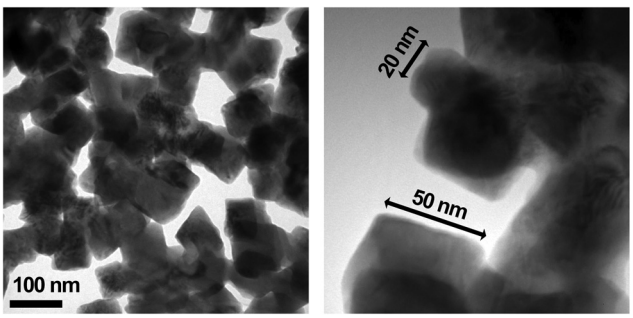

Fig. 9 TEM images of Bi_2Te_3 nanoparticles as obtained by reaction of $Bi(NMe_2)_3$ and $Te(SiEt_3)_2$ (2 : 3 molar ratio) in DIPB at 100 °C.

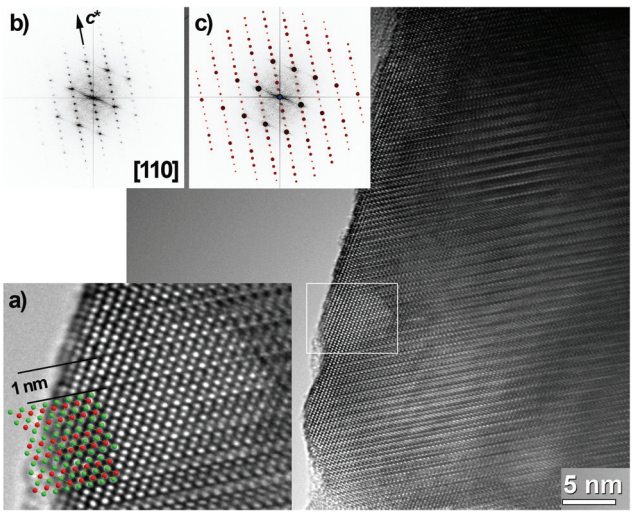

Fig. 10 HRTEM image of a Bi_2Te_3 nanoparticle from $Bi(NMe_2)_3$ and $Te(SiEt_3)_2$ (2 : 3 molar ratio) in DIBP at 100 °C. (a) Zoom of the boxed area with structure model as overlay; (b) Fourier transform of the whole HRTEM image; (c) FT with simulation of the diffraction pattern in [110] as overlay.

the stacking of the five membered Bi_2Te_3 building units. The contrasts in the image change strongly with increasing thickness as common in HRTEM, but the Fourier transform of the whole image shown in Fig. 10b) indicates that the periodicity is perfect. The Fourier transform matches perfect with the simulation of the electron diffraction for Bi_2Te_3 (Fig. 10c), and as no additional peaks or streaking is observed, an intergrowth of different phases of the Bi–Te system can be excluded. A closer inspection of the thin areas of the sample shows periodic 1 nm stacks perpendicular to the *c*-axis of Bi_2Te_3. Each of the stacks has five rows of well resolved contrast maxima, which match the positions of the atoms of Bi_2Te_3 in this projection. This is illustrated by an overlay of a ball and stick plot of Bi_2Te_3 in the same orientation and proofs the synthesis of pure Bi_2Te_3 (Fig. 10a).

Variation of the Bi-precursor. Since the reaction of $Bi(NMe_2)_3$ **4** and $Te(SiEt_3)_2$ yielded phase-pure Bi_2Te_3, we expanded our studies on analogous reactions of alternate bismuth triamides. $Bi(NEt_2)_3$ **5** as well as the asymmetric $Bi(NMeEt_2)_3$ **6** were chosen, which are oily liquids at ambient temperature, while **4** is a solid. The reaction of **5** and **6** with $Te(SiEt_3)_2$ at ambient temperature in THF-d_8 were monitored by ^{1}H-NMR spectroscopy. Compared to the reaction of **4**, which is finished after 15 min, the reaction of **5**, which proceeds with formation of the expected elimination product *N*,*N*-diethylamino-triethylsilane, is decelerated and incomplete even after 20 h (ESI, Fig. X†). Surprisingly, **6** didn't show any reaction at ambient temperature even after 20 h (Fig. S9†). One the basis of the NMR results, **5** and **6** are less suitable bismuth precursors for the synthesis of bismuth telluride nanoparticles than **4**.

Finally, we investigated the reaction of $BiCl_3$ with $Te(SiEt_3)_2$, which was expected to proceed with elimination of Et_3SiCl (dehalosilylation reaction). Since $BiCl_3$ is not soluble in non-coordinating solvents such as DIPB, we used oleylamine (OA) as solvent. The thermolysis reaction was performed at 160 °C for 14 h. The SEM of the resulting product showed very small particles without defined structure (Fig. S17†). The Bi : Te ratio (42 at% : 58 at%) is close to the expected value for Bi_2Te_3. These results were confirmed by PXRD, which proved the formation of Bi_2Te_3 as the only crystalline product (Fig. 11). The lattice parameters for the Bi_2Te_3 particles (a = 4.405(1) Å and c = 20.284(4) Å) are in good agreement with values reported in the literature for Bi_2Te_3 (JCPDS No. 015-0863).

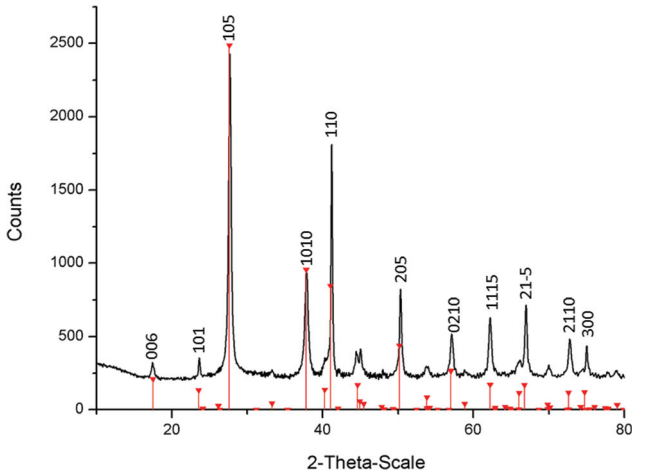

Fig. 11 X-ray diffractogram of the material as obtained by reaction of $BiCl_3$ and $Te(SiEt_3)_2$ in OA at 160 °C and reference (red: Bi_2Te_3, JCPDS 015-0863).

Experimental

Synthetic procedures, materials and methods

PVP* (Sigma-Aldrich) was used as received while 1,3-diisopropylbenzene (DIPB, Sigma-Aldrich) was carefully dried over Na/K alloy and oleylamine (OA, Acros) was degassed prior to use. $(Et_2Bi)_2Te$,[35] $Te(SiEt_3)_2$,[36] Et_4Bi_2,[37] Et_2Te_2,[38] $Bi(NMe_2)_3$,[39] $Bi(NEt_2)_3$ and $Bi(NEtMe)_3$ [40] were synthesized according to literature methods. All synthetic steps were performed under argon atmosphere using standard Schlenk techniques.

Thermolysis of $(Et_2Bi)_2Te$ 1. 200 mg (0.3 mmol) $(Et_2Bi)_2Te$ were dissolved in 10 mL of DIPB. The solution was heated to 80 °C for 14 h. 10 mL of MeOH were added after cooling the solution to ambient temperature and the precipitate was isolated by centrifugation and purified by repeated washing with chloroform (2–3 times). Yield: 53 mg (28% based on Bi content in **1**) Bi_4Te_3.

Thermolysis of $Et_2BiTeEt$ 2. 106.8 mg (0.2 mmol) Et_4Bi_2 and 62.7 mg (0.3 mmol) Et_2Te_2 were dissolved in either 15 mL of DIPB or OA at ambient temperature. Attempts to increase the Te content were performed with 15.4 mg (0.03 mmol) of TOPTe (Te excess of 15%). The red solution was heated to 100 °C and stirred at this temperature for either 3 or 14 h. The black solid was isolated as described before. Yield: 55 mg (55.4% based on Bi content in **2**) Bi_2Te.

Thermolysis of $Bi(NMe_2)_3$ and $Te(SiEt_3)_2$

Influence of reaction temperature. 53.6 mg (0.15 mmol) $Te(SiEt_3)_2$ were added to a yellow solution of 31.5 mg (0.1 mmol) $Bi(NMe_2)_3$ in 15 mL of DIPB, immediately yielding a greenish suspension. This suspension was heated to the desired temperature and stirred for 3 h at this temperature. After cooling to ambient temperature, 10 mL of MeOH were added and the black solid was separated from the liquid by centrifugation and repeatedly washed with chloroform (2–3 times). Biphasic mixtures of Bi_2Te_3 (major phase, >95% according to PXRD) and Bi_4Te_3 in different molar ratios depending on the reaction temperature were obtained.

Influence of precursor ratio. A solution of 107.4 mg (0.3 mmol) $Te(SiEt_3)_2$ in 15 mL of DIPB was heated to 100 °C and a solution of either 68.2 mg (0.2 mmol), 102.4 mg (0.3 mmol) or 136.5 mg (0.4 mmol) $Bi(NMe_2)_3$ in 2 mL of DIPB was added to the hot solution (hot injection method). The resulting black suspension was stirred at 100 °C for 3 h. After cooling to ambient temperature, 10 mL of MeOH were added and the solid was isolated from the solution by centrifugation

and washed with chloroform (2–3 times). **Bi_2Te_3:** yield: 79.9 mg (0.094 mmol, 94%); **BiTe:** yield: 96.9 mg (0.29 mmol, 96%); **Bi_4Te_3:** yield: 114 mg (0.093 mmol, 93%).

Influence of Bi-precursor. 107.4 mg (0.3 mmol) $Te(SiEt_3)_2$ and either 87.1 mg (0.2 mmol) $Bi(NEt_2)_3$ or 76.7 mg (0.2 mmol) $(Bi(NEtMe)_3$, respectively, were dissolved in 15 mL of DIPB and heated to 120 °C. The solution was stirred for 3 h at this temperature. Due to the insolubility of $BiCl_3$ in DIPB, the thermolysis reaction of 63.1 mg (0.2 mmol) $BiCl_3$ and 107.4 mg (0.3 mmol) was performed in 15 mL of OA. The solution was heated to 160 °C for 3 h and the isolation and purification of the resulting black solid was performed as described before.

Characterization

X-ray powder diffraction (PXRD). PXRD patterns were obtained at ambient temperature (25 ± 2 °C) using a Bruker D8 Advance powder diffractometer in Bragg–Brentano mode with Cu K_α radiation (λ = 1.5418 Å, 40 kV, and 40 mA). The powder samples were investigated in the range of 5 to 90° 2θ with a step size of 0.01° 2θ and a counting time of 0.3 s. Rietveld refinement was performed with the program package TOPAS 4.2 from Bruker.

SEM analysis. Scanning electron microscopy (SEM) studies were carried out on a Jeol JSM 6510 equipped with an energy-dispersive X-ray spectroscopy (EDX) device (Bruker Quantax 400).

TEM analysis. TEM studies were conducted on transmission electron microscopes (i) FEI Philips CM30 T/LaB_6 operated at 300 kV and (ii) FEI-Philips CM300 UT/FEG operated at 300 kV. Both microscopes are equipped Gatan CCD's for image recording and with Thermo NSS systems for EDS analysis using a Si(Li) Nanotrace and a HP-Ge EDS detector, respectively. The samples were prepared on perforated carbon foils without further grinding.

Conclusions

We investigated the suitability of two possible *single source precursors*, $(Et_2Bi)_2Te$ **1** and $Et_2BiTeEt$ **2**, for the solution-based synthesis of Bi_2Te_3 nanoparticles. The thermal decomposition pathways of both precursors were elucidated by ^{1}H-NMR spectroscopy and differential scanning calorimetry (DSC). Thermolysis of **1** in DIPB led to the formation of Bi_4Te_3 at 80 °C and mixtures of Bi_4Te_3 and elemental Bi at higher temperatures, while thermolysis of *in situ* generated **2** in DIPB or OA gave pseudo-cubic Bi_2Te particles, whose size increase with increasing reaction time. To the best of our knowledge, this is the first report of the solution based formation of Bi_2Te. For all thermolysis reactions, the formation of tellurium poor phases were observed. **1** and **2** are therefore unsuitable for the synthesis of Bi_2Te_3, which may be attributed to the comparable low Te–Bi binding energy and complex decomposition mechanism. We assume that the formation of temperature stable Et_2Te is an efficient process for the transport of Te out of the reaction mixture, leading to Te-poor (Bi-rich) materials.

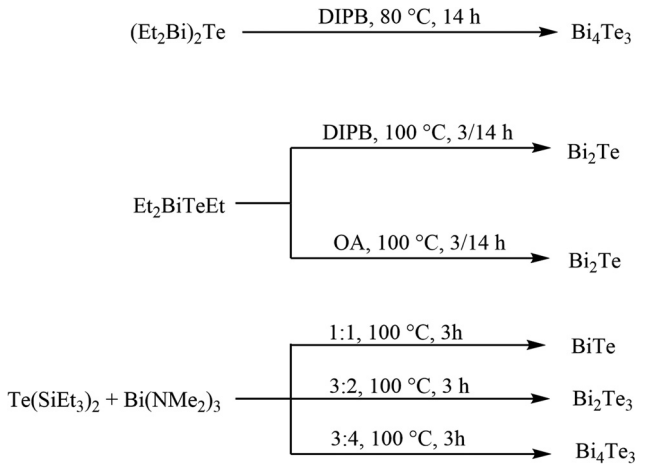

Fig. 12 Summary of the ideal reaction conditions for the formation of phase-pure binary bismuth–tellurium materials.

In contrast to the *single source precursors*, the *dual source approach* using the reaction of $Te(SiEt_3)_2$ and $Bi(NMe_2)_3$ was successfully applied for the synthesis of multiple Bi–Te phases including Bi_2Te_3 depending on the precursor ratio. In contrast, analogous reactions of $Bi(NEt_2)_3$ and $Bi(NMeEt)_3$ occurred with formation of a mixture of elemental tellurium and bismuth and a mixture of Bi_4Te_3 and tellurium, respectively, while the reaction of $BiCl_3$ and $Te(SiEt_3)_2$ gave Bi_2Te_3 nanoparticles. The reaction conditions leading to phase pure material are summarized in Fig. 12.

Acknowledgements

S. Schulz thanks the Deutsche Forschungsgemeinschaft (DFG) for financial support of this work within the priority program SPP 1708 (Material Synthesis near Room Temperature).

Notes and references

1 M. H. Elsheikh, D. A. Shnawah, M. F. M. Sabri, S. B. M. Said, M. H. Hassan, M. B. A. Bashir and M. Mohamad, *Renewable Sustainable Energy Rev.*, 2014, **30**, 337.
2 (*a*) D. M. Rowe, *CRC Handbook of Thermoelectrics*, CRC Press, Boca Raton, FL, 1995; (*b*) J. R. Drabble and C. H. L. Goodman, *J. Phys. Chem. Solids*, 1958, **5**, 142.
3 Z. Wang, J. E. Alaniz, W. Jang, J. E. Garay and C. Dames, *Nano Lett.*, 2011, **11**, 2206.
4 M. Scheele, N. Oeschler, I. Veremchuk, K.-G. Reinsberg, A.-M. Kreuziger, A. Kornowski, J. Broekaert, C. Klinke and H. Weller, *ACS Nano*, 2010, **4**, 4283.
5 V. Stavila, D. B. Robinson, M. A. Hekmaty, R. Nishimoto, D. L. Medlin, S. Zhu, T. M. Tritt and P. A. Sharma, *ACS Appl. Mater. Interfaces*, 2013, **5**, 6678.
6 L. Chen, Q. Zhao and X. Ruan, *Mater. Lett.*, 2012, **82**, 112.

7 R. J. Mehta, Y. Zhang, C. Karthik, B. Singh, R. W. Siegel, T. Borca-Tasciuc and G. Ramanath, *Nat. Mater.*, 2012, **11**, 233.
8 (*a*) K. Knapas, T. Hatanpää, M. Ritala and M. Leskelä, *Chem. Mater.*, 2010, **22**, 1386; (*b*) S. Zastrow, J. Gooth, T. Boehnert, S. Heiderich, W. Toellner, S. Heimann, S. Schulz and K. Nielsch, *Semicond. Sci. Technol.*, 2013, **28**, 035010; (*c*) C. Bae, T. Bohnert, J. Gooth, S. Lim, S. Lee, H. Kim, S. Heimann, S. Schulz, H. Shin and K. Nielsch, *Semicond. Sci. Technol.*, 2014, **29**, 064003.
9 S. Schulz, S. Heimann, K. Kaiser, O. Prymak, W. Assenmacher, J. T. Brüggemann, B. Mallik and A.-V. Mudring, *Inorg. Chem.*, 2013, **52**, 14326.
10 (*a*) T. J. Groshens, R. W. J. Gedridge and C. K. Lowe-Ma, *Chem. Mater.*, 1994, **6**, 727; (*b*) T. Groshens, R. Gedridge, R. Scheri and T. Cole, in Fifteenth International Conference on Thermoelectrics Proceedings ICT '96, IEEE, 1996, p. 430.
11 Z. Stary, J. Horak, M. Stordeur and M. Stölzer, *J. Phys. Chem. Solids*, 1988, **49**, 29.
12 J. W. G. Bos, H. W. Zandbergen, M.-H. Lee, N. P. Ong and R. J. Cava, *Phys. Rev. B: Condens. Matter*, 2007, **75**, 195203.
13 (*a*) M. A. Malik, M. Afzaal and P. O'Brien, *Chem. Rev.*, 2010, **110**, 4417; (*b*) H. J. Gysling, A. A. Wernberg and T. N. Blanton, *Chem. Mater.*, 1992, **4**, 900.
14 (*a*) J. S. Ritch, T. Chivers, M. Afzaal and P. O'Brien, *Chem. Soc. Rev.*, 2007, **36**, 1622; (*b*) P. L. Musetha, N. Revaprasadu, G. A. Kolawole, R. V. S. R. Pullabhotla, K. Ramasamy and P. O'Brien, *Thin Solid Films*, 2010, **519**, 197; (*c*) N. O. Boadi, M. Azad Malik, P. O'Brien and J. A. M. Awudza, *Dalton Trans.*, 2012, **41**, 10497; (*d*) K. Yu, X. Liu, Q. Zeng, M. Yang, J. Ouyang, X. Wang and Y. Tao, *Angew. Chem., Int. Ed.*, 2013, **52**, 11034.
15 (*a*) N. Maiti, S. H. Im, C.-S. Lim and S. I. Seok, *Dalton Trans.*, 2012, **41**, 11569; (*b*) F. T. F. O'Mahony, U. B. Cappel, N. Tokmoldin, T. Lutz, R. Lindblad, H. Rensmo and S. A. Haque, *Angew. Chem., Int. Ed.*, 2013, **52**, 12047; (*c*) J. R. Castro, K. C. Molloy, Y. Liu, C. S. Lai, Z. Dong, T. J. White and E. R. T. Tiekink, *J. Mater. Chem.*, 2008, **18**, 5399; (*d*) M. Bochmann, X. Song, M. B. Hursthouse and A. Karaulov, *J. Chem. Soc., Dalton Trans.*, 1995, 1649; (*e*) H.-W. Chang, B. Sarkar and C. W. Liu, *Cryst. Growth Des.*, 2007, **7**, 2691; (*f*) W. Lou, M. Chen, X. Wang and W. Liu, *Chem. Mater.*, 2007, **19**, 872; (*g*) R. K. Sharma, G. Kedarnath, V. K. Jain, A. Wadawale, M. Nalliath, C. G. S. Pillai and B. Vishwanadh, *Dalton Trans.*, 2010, **39**, 8779.
16 S. S. Garje, D. J. Eisler, J. S. Ritch, M. Afzaal, P. O'Brien and T. Chivers, *J. Am. Chem. Soc.*, 2006, **128**, 3120.
17 G. Gupta and J. Kim, *Dalton Trans.*, 2013, **42**, 8209.
18 S. L. Benjamin, C. H. de Groot, A. L. Hector, R. Huang, E. Koukharenko, W. Levason and G. Reid, *J. Mater. Chem. C*, 2015, **3**, 423.
19 R. S. Dickson and K. D. Heazle, *J. Organomet. Chem.*, 1995, **493**, 189.
20 S. Schulz, S. Heimann, J. Friedrich, M. Engenhorst, G. Schierning and W. Assenmacher, *Chem. Mater.*, 2012, **24**, 2228.
21 G. Bendt, S. Schulz, S. Zastrow and K. Nielsch, *Chem. Vap. Deposition*, 2013, **19**, 235.
22 S. L. Benjamin, C. H. de Groot, C. Gurnani, A. L. Hector, R. Huang, E. Koukharenko, W. Levason and G. Reid, *J. Mater. Chem. A*, 2014, **2**, 4865.
23 S. Heimann, D. Bläser, C. Wölper and S. Schulz, *Organometallics*, 2014, **33**, 2295.
24 P. A. Stadelmann, *JEMS electron microscopy software java version 3*.
25 K. Yamana, K. Kihara and T. Matsumoto, *Acta Crystallogr., Sect. B: Struct. Crystallogr. Cryst. Chem.*, 1979, **35**, 147.
26 S. Heimann, A. Kuczkowski, D. Bläser, C. Wölper, R. Haak, G. Jansen and S. Schulz, *Eur. J. Inorg. Chem.*, 2014, 4858.
27 M. Wieber and I. Sauer, *Z. Naturforsch., B: Chem. Sci.*, 1987, **42**, 695.
28 H. J. Breunig and D. Müller, *Z. Naturforsch., B: Anorg. Chem. Org. Chem.*, 1986, **41**, 1129.
29 L. Pauling and D. M. Yost, *Proc. Natl. Acad. Sci. U. S. A.*, 1932, **18**, 414; L. Pauling, *J. Am. Chem. Soc.*, 1932, **54**, 3570.
30 S. Ishida, F. Hirakawa, K. Furukawa, K. Yoza and T. Iwamoto, *Angew. Chem., Int. Ed.*, 2014, **53**, 11172.
31 (*a*) A. J. Ashe III, E. G. Ludwig and J. Oleksyszyn, *Organometallics*, 1983, **2**, 1859; (*b*) F. Calderazzo, R. Poli and G. Pellini, *Dalton Trans.*, 1984, 2365.
32 (*a*) H. J. Breunig, *Phosphorus, Sulfur Silicon Relat. Elem.*, 1988, **38**, 97; (*b*) H. J. Breunig and S. Gülec, *Z. Naturforsch., B: Anorg. Chem. Org. Chem.*, 1986, **41**, 1387; (*c*) S. Schulz, *Coord. Chem. Rev.*, 2015, **297–298**, 49.
33 M. Bochmann, X. Song, M. B. Hursthouse and A. Karaulov, *Dalton Trans.*, 1995, 1649.
34 S. Nakajima, *J. Phys. Chem. Solids*, 1963, **24**, 479.
35 H. J. Breunig, K. H. Ebert and R. E. Schulz, *Z. Naturforsch., B: Chem. Sci.*, 1995, **50**, 735.
36 M. R. Detty and M. D. Seidler, *J. Org. Chem.*, 1982, **47**, 1354.
37 R. King and J. Eisch, *Organometallic Syntheses*, Elsevier, Amsterdam, 1986, vol. 3.
38 K. Hamada and H. Morishita, *Synth. React. Inorg. Met.-Org. Chem.*, 1981, **11**, 597.
39 F. Ando, T. Hayashi, K. Ohashi and J. Koketsu, *J. Inorg. Nucl. Chem.*, 1975, **37**, 2011.
40 M. Vehkamäki, T. Hatanpää, M. Ritala and M. Leskelä, *J. Mater. Chem.*, 2004, **14**, 3191.

